

# Dependence of Star Formation Activity On Stellar Mass and Environment From the Redshift One LDSS-3 Emission Line Survey (ROLES)

I.H. Li<sup>1,\*</sup>, Karl Glazebrook<sup>1</sup>, David Gilbank<sup>2</sup>, Michael Balogh<sup>2</sup>, Richard Bower<sup>3</sup>, Ivan Baldry<sup>4</sup>, Greg Davies<sup>3</sup>, George Hau<sup>1</sup> and Pat McCarthy<sup>5</sup>

<sup>1</sup>Centre for Astrophysics & Supercomputing, Swinburne University of Technology, PO Box 218, Hawthorn, Victoria 3122, Australia

<sup>2</sup>Department of Physics and Astronomy, University of Waterloo, Waterloo, Ontario, Canada, N2L 3G1

<sup>3</sup>Institute for Computational Cosmology, Department of Physics, University of Durham, South Road, Durham, DH1 3LE, UK

<sup>4</sup>Astrophysics Research Institute, Liverpool John Moores University, Twelve Quays House, Egerton Wharf, Birkenhead Ch41 1LD, UK

<sup>5</sup>Carnegie Observatories, 813 Santa Barbara Street, Pasadena, California, 91101 USA

\*email: tli@astro.swin.edu.au

14 June 2018

## ABSTRACT

Using the sample from the *Redshift One LDSS3 Emission line Survey* (ROLES), we probe the dependence of star formation rate (SFR) and specific star formation rate (sSFR) as a function of stellar mass  $M_*$  and environment as defined by local galaxy density, in the CDFS field. Our spectroscopic sample consists of 312 galaxies with  $K_{AB} < 24$ , corresponding to stellar mass  $\log(M_*/M_\odot) > 8.5$ , and with [OII] derived star-formation rates  $\text{SFR} > 0.3M_\odot/\text{yr}$ , at  $0.889 \leq z \leq 1.149$ . The results have been compared directly with the Sloan Digital Sky Survey Stripe 82 sample at  $0.032 \leq z \leq 0.05$ . For star-forming galaxies, we confirm that there is little correlation between SFR and density at  $z \sim 0$ . However, for the lowest mass galaxies in our  $z \sim 1$  sample, those with  $\log(M_*/M_\odot) < 10$ , we find that both the median SFR and specific SFR *increase* significantly with increasing local density. The “downsizing” trend for low mass galaxies to be quenched progressively later in time appears to be more pronounced in moderately overdense environments. Overall we find that the evolution of star-formation in galaxies is most strongly driven by their stellar mass, with local galaxy density playing a role that becomes increasingly important for lower mass galaxies.

**Key words:** galaxies: evolution, stellar content

## 1 INTRODUCTION

The observed correlation between stellar mass and star formation rate (SFR) in galaxies as a function of redshift provides insight into the integrated SFR over the history of the Universe (e.g. Bell et al. 2007; Noeske et al. 2007b). Several independent observations now suggest that the SFR in galaxies is regulated and in some cases quenched by different physical processes (e.g. Peng et al. 2010). One of the fundamental questions is whether these processes are more closely correlated with internal galaxy properties (such as mass and luminosity) or with their external environment.

In particular, many studies have shown that the SFR in individual galaxies is affected by environment. In the local Universe, it is well established that the fraction of passive (red) galaxies is higher in regions of high galaxy density, while regions of low galaxy density harbor predominantly blue, star forming galaxies (e.g., Dressler 1980; Balogh et al. 2004; Baldry et al. 2006; Pannella et al. 2009; Bamford et al. 2009). This is also, perhaps more directly, reflected in the star formation rates of the galax-

ies (e.g., Lewis et al. 2002; Gómez et al. 2003; Hogg et al. 2004). Interestingly, it is primarily the fraction of star forming galaxies that correlates with environment (e.g., Baldry et al. 2006; Li et al. 2009; Iovino et al. 2010; Peng et al. 2010); the distribution of colours or SFR among the active population itself seems surprisingly independent of environment, at least at low redshift (e.g., Balogh et al. 2004; Yee et al. 2005; Carter et al. 2001; Rines et al. 2005; Cassata et al. 2007; Balogh et al. 2009). This may suggest that any environmental influence responsible for quenching SFR must operate on a short time scale of few Gyrs (e.g., Balogh et al. 2004; von der Linden et al. 2010).

It is also well established that the global SFR density ( $\rho_{SFR}$ ) has decreased steadily from  $z \sim 1$  to  $z \sim 0$  (e.g., Lilly et al. 1996; Madau et al. 1996; Hopkins et al. 2004). The contribution of galaxies to  $\rho_{SFR}$  depends on their stellar mass, with massive galaxies at higher-redshifts contributing a greater total  $\rho_{SFR}$  than similar mass galaxies today. This picture has been labeled ‘downsizing’ — the term denotes the general empirical observation that

arXiv:1010.1447v1 [astro-ph.CO] 7 Oct 2010

star-formation activity progresses from higher mass to lower mass systems with cosmic time (Cowie et al. 1996). There are various manifestations of this effect. For example, Juneau et al. (2005) and Mobasher et al. (2009) found that massive galaxies contributed a greater proportion of  $\rho_{SFR}$  at high redshifts. Recently many surveys such as GOODS (e.g., Santini et al. 2009; Magnelli et al. 2009), GDDS (e.g., Abraham et al. 2004; Juneau et al. 2005), K20 (e.g., Cimatti et al. 2002; Daddi et al. 2002), DEEP (e.g., Vogt et al. 2005), and zCOSMOS (e.g., Lilly et al. 2007; Pozzetti 2009; Cucciati 2010) have confirmed that stellar mass plays a fundamental role in determining the fate of a galaxy.

With large, spectroscopic surveys, several of these studies have begun to explore the effect of environment over a wide range of redshifts (e.g. Cooper et al. 2008; Cooper et al. 2010; Maier 2009; Peng et al. 2010; Iovino et al. 2010; Vulcani et al. 2010; Cucciati 2010), and they generally find that environment is a second-order effect compared with the mass-driven evolution. Peng et al. (2010) has proposed a particularly interesting, empirical model in which environment induces transformation from active to passive, at a rate that is surprisingly independent of stellar mass.

Since environmental influences might be expected to have the largest effect on gas-rich, low-mass galaxies, the relevant physics may thus best be probed by studying such galaxies at  $z = 1$  or higher. This is a particularly interesting epoch, as there is mounting evidence that star formation may actually be *enhanced* in gas-rich galaxies that live in dense regions at these redshifts (e.g., Elbaz et al. 2007; Muzzin et al. 2008; Cooper et al. 2008; Ideue et al. 2009; Sobral et al. 2010), although the fraction of red (passively-evolving) galaxies still increases with density (e.g. Cooper et al. 2010). However, most of the results cited above are based on flux-limited surveys, and hence can only spectroscopically probe the high-mass regime ( $> 10^{10} M_{\odot}$ ) at  $z \sim 1$ . For a complete picture it is necessary to probe SFR in low-mass galaxies as well.

We have therefore carried out a spectroscopic survey, the ‘Redshift One LDSS3 Emission line Survey’ (ROLES), to study the dependence of  $\rho_{SFR}$  on stellar mass at  $z \sim 1$ . Our observations focus on low-mass galaxies ( $8.5 \leq \log(M_*/M_{\odot}) \leq 10$ ),  $\sim 10$  times less massive than those typically considered in the current literature. We aim to obtain a sample complete in both SFR and stellar mass. The first two papers of this series, Davies et al. (2009) and Gilbank et al. (2010b) (hereafter Paper I and Paper II), revealed that the  $\rho_{SFR}$  does not increase continuously with decreasing stellar mass, but instead exhibits a ‘turn-over’ at  $\sim 10^{10} M_{\odot}$  just as it does in the local Universe. This demonstrates that low mass galaxies do not dominate the total SFR density at any epoch  $z \leq 1$ . Comparing the results with those derived from SDSS galaxies at  $z \sim 0$  using an identical [OII] calibration, Paper II finds that the shape of the total SFR density as a function of stellar mass remains similar at  $z \sim 1$  and  $z \sim 0$ , although the magnitude of the total SFR density becomes smaller at  $z \sim 0$ . This implies that the rate at which the SFR density decreases is not a strong function of stellar mass. In other words, the evolution of global  $\rho_{SFR}$  is better described as a simple evolution of the normalization of  $\rho_{SFR}(M_*)$ , and the shape and relative contributions of galaxies of different masses remained unchanged.

In this paper, we address the star-forming population of galaxies at  $z \sim 1$ , and use ROLES to probe how SFR correlates with environment at the lowest stellar masses considered to date. The structure of the paper is as follows. We present our survey data and catalogues in §2. The environmental measure, local galaxy density, is presented in §3; we test our measurement on local data from the

SDSS to show that it provides a robust tracer of environment. We present the results in §4, and discuss the implications and limitations of this work in §5.

## 2 DATA

### 2.1 Low mass galaxies from ROLES

In Papers I and II, we have constructed a sample of star forming galaxies with stellar mass between  $10^{8.5}$  and  $10^{10} M_{\odot}$  at  $z \sim 1$  using the [OII] $\lambda 3727$  emission line luminosity to derive the SFR. For a single galaxy [OII] is not an ideal SFR tracer, but it has been established that, on average, it traces the SFR derived from dust-corrected  $H_{\alpha}$  luminosities (e.g., Jansen et al. 2001; Kewley et al. 2004; Gilbank et al. 2010a). With reasonable assumptions about dust and metallicity, we can statistically compare [OII] selected sample in different regimes of stellar mass and environments.

The observations were conducted using the LDSS3 on the 6.5m Magellan at Las Campanas, in nod& shuffle (Glazebrook & Bland-Hawthorn 2001) mode. The full design of the spectroscopic survey and details of the data reduction and methodology used are given in Paper II, and we briefly recap the most significant points here. We use a red blazed 300 l/mm grism with an average dispersion of  $\sim 2.7 \text{ \AA}$  per pixel. Our custom KG750 filter has a 7040-8010 $\text{ \AA}$  bandpass, and hence allows us to observe [OII] $\lambda 3727$  over  $z=0.889-1.149$ . The 8 arcmin LDSS3 field of view typically allows us to allocate almost  $\sim 200$  non-overlapping 3 arcsec long slits in this configuration using nod & shuffle mode.

We observed six masks in each of three pointings; two within the GOODS-CDFS, and a third in the FIRES MS1054 field. These fields were chosen because they have very deep  $K$ -band data and publicly available photometric-redshift catalogues. Our GOODS-CDFS parent catalog was kindly provided by Mobasher et al. (2004), and the MS1054 catalog was obtained from the FIRES team (Förster Schreiber et al. 2006). We prioritized galaxies with photometric-redshifts which indicate the greatest probability that the [OII] line lies in our redshift range. A full discussion of the selection and completeness can be found in Paper II, and we revisit the completeness for our purposes in Section 2.5.

Following Paper II, we select emission line objects with greater than  $4\sigma$  significance, and with a high likelihood that the line is [OII] rather than something else, based on the photometric redshift probability. This leaves us with 311 [OII] galaxies with spectroscopic redshifts from the CDFS and FIRES patches. Although both fields are statistically equivalent, the smaller FIRES field only contributes 75 galaxies to the whole sample. Moreover, our analysis will need to combine our spectroscopic sample with the publicly available CDFS redshift data for brighter, higher mass galaxies to allow us to accurately measure local environment. Unfortunately, equivalent data are not available for the FIRES field in our redshift range. For these reasons, we choose to omit data from the FIRES field from the present analysis.

In Paper II, we tested and discussed the derivation of SFR using several different methods. In this paper, we will convert [OII] luminosity to SFR using the empirical, mass-dependent correction introduced in Gilbank et al. (2010a). In brief, our SFR is estimated from the Kennicutt (1998) relation, converted to the Baldry & Glazebrook (2003) IMF and with a mass-dependent correction that accounts for variations in dust, metallicity or other effects with mass. The typical derived SFR is  $\sim 1 M_{\odot}/\text{yr}$  at  $0.889 \leq z \leq 1.149$ , and our sample is complete to SFR  $\sim 0.3 M_{\odot}/\text{yr}$ .

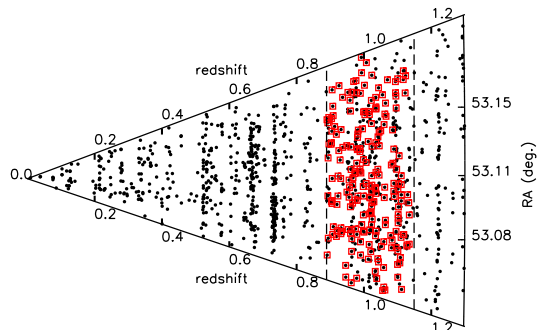


**Figure 1.** The spectroscopic redshift distribution of the 1381 galaxies in our CDFS spectroscopic sample. The sample is generated by combined our LDSS3 spectra with publicly available data as described in the text. The vertical, dashed lines mark our LDSS3 redshift window,  $0.889 \leq z \leq 1.149$ , and the red squares mark LDSS3 galaxies in this redshift range. A total of 441 spectroscopic galaxies are within this redshift window.

We note that AGN are rare in our sample (Paper IV; Gilbank et al., in prep), as expected due to their low stellar mass (e.g., Kauffmann et al. 2003b; Kauffmann et al. 2004). This calibration is based on a nearby sample of galaxies from SDSS, and will account for any systematic effect (e.g. dust or metallicity) that depends only on stellar mass. In applying this calibration to our present sample, we make a fundamental assumption that it is also applicable to galaxies at  $z \sim 1$ . Since our main purpose is to compare galaxies of fixed stellar mass, in different environments, our main results are insensitive to this assumption. They are, however, dependent on the assumption that the dust content and metallicity of a galaxy are primarily determined by its stellar mass, and not by some other parameter that correlates with environment.

## 2.2 Additional Redshifts

For the GOODS-CDFS field, the public spectra are obtained from ESO FORS2 observations (v3.0) of Vanzella et al. (2005, 2006, 2008). These targets were selected to have  $z_{850} < 26$ , with  $(i_{775} - z_{850}) > 0.6$  for the primary targets and  $(i_{775} - z_{850}) < 0.6$  for the secondary. We only include those galaxies with a good spectroscopic flag (as ‘A’ or ‘B’) in our spectroscopic catalog, using a  $0.5''$  matching criterion in position. This gives us a total of 516 FORS2 spectra. We compute the [OII] flux from these spectra, and use the method described in § 2.1 to derive the SFR. We also use redshifts from FIREWORKS (Wuyts et al. 2008), which provide 2119 spectroscopic redshifts obtained from various sources in the literature. We match these redshifts to our photometric catalogue using a radius of  $0.5''$ , and find 1463 of them within our two LDSS3 pointings, and with spectroscopic quality confidence  $z_{qop} \geq 0.5$ . Unfortunately, we do not have [OII] measurements for these spectra; the redshifts will be useful for measuring the local density in our fields, but will not contribute to the SFR measurement. We will account for this in our weighting scheme, described below.

## 2.3 Final Spectroscopic Catalogue and Stellar Masses

Our final catalog contains 1381 galaxies with multiwavelength optical and near-infrared photometry, and confident spectroscopic redshifts. Among the 441 galaxies at  $0.889 \leq z \leq 1.149$ , 312 have an available SFR measurement (i.e. from the LDSS3 and FORS2 subsets). The distribution of spectroscopic redshifts of our final catalog is shown in Fig. 1. We estimate the stellar mass for individual galaxies using the spectral energy distribution grid fitting method of Glazebrook et al. (2004), as in Paper II. We note that the ‘stellar mass’ as defined here refers to the mass currently locked in stars, which is less than the ‘formed stellar mass’, as it excludes recycled gas and mass locked in sub-stellar compact remnants. The median stellar mass  $M_*$  for galaxies with  $22.5 \leq K \leq 24.0$  at  $0.889 \leq z \leq 1.149$  is  $\log(M_*/M_\odot) \sim 9.1$ , and the limit for our sample of star-forming galaxies is  $\log(M_*/M_\odot) = 8.5$ . In the rest of this paper we refer to this combined spectroscopic catalog in the CDFS field (LDSS3+FORs2+FIREWORKS) as ‘ROLES’ and those emission galaxies obtained in our own LDSS3 survey as ‘LDSS3’ galaxies.

## 2.4 The Photometric-Redshift Catalogs

We use photometric redshifts (hereafter ‘photo- $z$ ’) to estimate the completeness, in both SFR and redshifts, of our sample (see §2.5). The public photo- $z$  catalog is obtained from FIREWORKS (Wuyts et al. 2008), who used a standard template fitting method. The  $1\sigma$  uncertainty in these photo- $z$ , compared with spectroscopic redshifts, is 0.074 at  $z < 2$  over all magnitudes; and 0.061 and 0.114 for galaxies with  $K < 22.5$  and  $22.5 \leq K \leq 24.0$ , respectively. For the few galaxies in our ROLES catalogue that do not have FIREWORKS redshifts, we use the photo- $z$  from which our survey was initially selected, Mobasher et al. (2004), as described in Paper II.

Since the photo- $z$  are important for our completeness estimates, it is useful to check these using an independent method. Therefore, we derive our own independent photo- $z$ . This allows us to cross-check the stability of our the computation of local galaxy density, and hence the final results, against quite different photo- $z$  methods (Appendix A). These new photo- $z$  are calculated using an empirical fitting method modified from Li & Yee (2008). This requires a training set, which we construct using the full spectroscopic catalogue in the CDFS field, including our LDSS3 targets. We modify the method of Li & Yee (2008) so that, instead of using 19 fixed magnitude-color cells to derive the fitting solutions, we do the fit using a subset of training-set galaxies which are chosen to have magnitudes and colors closest to a galaxy for which we wish to measure a photo- $z$ . This reduces the bias in the fitting solutions when a galaxy is located near the edge of a color-magnitude cell. During the fitting process, a weight based on the rank of the quadratic sum of magnitudes and colors to the input galaxy is assigned to each training set galaxy in the same dynamical magnitude-color subset; i.e., the training-set galaxies with magnitudes and colors more similar to the input galaxies contribute more weight. The photo- $z$  PDF and hence uncertainty for each galaxy is computed by simulating galaxy photometry uncertainties with Gaussian distributions, and bootstrapping the training-set galaxies in a magnitude-color cell. Our modified photo- $z$  method has been tested in Hildebrandt (2010), and has shown robust results in both tests using the mock data and observed GOODS-N data. The  $1\sigma$  dispersions are 0.040 and 0.114 using the empirical photo- $z$  for galaxies with  $K < 22.5$  and  $22.5 \leq K \leq 24.0$ , respectively.

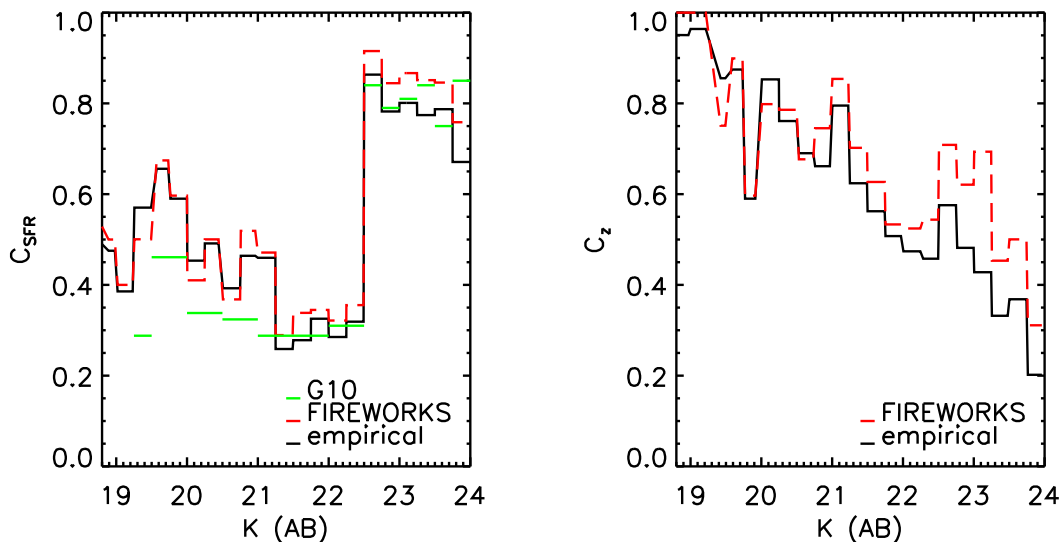


**Figure 2.** Our survey completeness as a function of apparent  $K(AB)$  in a binsize of  $\Delta K=0.25$  in our survey. The left panel shows  $C_{SFR}$ , which represents the fraction of galaxies for which we have available star formation rate measurements. The right panel shows  $C_z$ , which is our redshift completeness. These estimates rely on the PDF of our photo- $z$  estimators. The (red) dashed curves are computed using the public FIREWORKS photo- $z$  catalogs, while the solid lines are derived using our empirical photo- $z$ . The use of different photo- $z$  largely affects  $C_z$  at  $22.5 \leq K \leq 24$ . The  $C_{SFR}$  from Paper II is overlotted as thin green bars (labelled G10).

All the science analyses in this paper have been done using both the public FIREWORKS and our empirical photo- $z$ . We find that the main difference is in the completeness measures (see §2.5), but our conclusions are insensitive to which set is used.

## 2.5 Completeness

Following Paper II, we derive *a posteriori* completeness corrections for our sample selection strategy, using the photo- $z$  probability distribution function (PDF) of each galaxy. If a galaxy has a reliable spectroscopic redshift, we replace its photo- $z$  PDF with a  $\delta$ -function located at the spectroscopic redshift. Since the public data compiled by FIREWORKS provide us with redshifts but not SFR, we must define two completeness corrections:  $C_z$  and  $C_{SFR}$ , respectively. The SFR completeness  $C_{SFR}$  is computed in bins of  $K$  magnitude, with a binsize  $\Delta K=0.25$  as,

$$C_{SFR}(K) = \frac{\sum_i \int_{0.889}^{1.149} P_i(z|slit) dz}{\sum_j \int_{0.889}^{1.149} P_j(z) dz}. \quad (1)$$

The denominator is the sum of the photo- $z$  PDF of all the galaxies in a  $K$  magnitude bin over our redshift range  $0.889 \leq z \leq 1.149$ . The numerator is computed as the sum of the photo- $z$  PDF over the same redshift range for the galaxies in the same  $K$  magnitude bin but with slits allocated from either our LDSS3 data or the FORS2 catalogue. This implicitly assumes that redshifts are successfully obtained for every targeted galaxy that has significant SFR and lies within the specified redshift range. This is likely a good approximation for our faint, LDSS3 sample (see below). Although the redshift success of the FORS2 spectroscopy is only about 70 per cent (Vanzella et al. 2008), we assume here that redshift failures are either absorption-line galaxies, or galaxies with  $z > 1.4$ , for which the [OII] line would not be accessible. A plot of  $C_{SFR}(K)$  as a function of magnitude is shown in Fig. 2. The

values are quite high ( $\sim 0.8$  in the range  $22.5 < K < 24$ ) as we observed nearly all the faint targets in our redshift range. For the LDSS3 subsample, this  $C_{SFR}(K)$  is analogous to what Paper II terms ‘ $w_k$ ’, which was used to calculate SFR densities (equation 15 of Paper II). We compare our completeness estimates with  $w_k$  directly in Fig. 2, and we find that the two completeness estimates are similar, but not identical. The main difference is due to the fact that  $w_z$  in Paper II also accounted for the 70% redshift success rate of the FORS2 spectra. This is the correct approach if the completeness is independent of SFR (i.e. emission line presence) and redshift, which seems unlikely. In any case, this makes little difference for any of our results.

When computing local densities, we can make use of all the spectroscopy, including those public redshifts for which [OII] is unavailable to us. In this case we consider a redshift completeness  $C_z$ , defined as

$$C_z(K) = \frac{\sum_i \int_{0.889}^{1.149} P_i(z_{spec}) dz}{\sum_j \int_{0.889}^{1.149} P_j(z) dz} = \frac{N(z_{spec} = 0.889 - 1.149)}{\sum_j \int_{0.889}^{1.149} P_j(z) dz}, \quad (2)$$

where now the numerator is a sum over all galaxies with spectroscopic redshifts. Because we assume a  $\delta$ -function redshift PDF for galaxies with spectroscopic redshifts, this is equivalent to the number of galaxies with spectro- $z$  within our redshift range. We show  $C_z$  in Figure 2. Note that  $C_z$  is larger than  $C_{SFR}$  at  $K < 22.5$ , because of the inclusion of public redshifts in FIREWORKS for which SFR measurements are unavailable.

Figure 2 shows that at the faintest magnitudes, where we have contributed new LDSS3 spectroscopy, the completeness  $C_{SFR} \sim 0.8$  is quite high, reflecting the high sampling completeness of our survey (Paper II). The fact that the redshift completeness  $C_z$  is also quite high ( $\sim 0.6$ ) at these magnitudes, indicates that the majority of these galaxies have ongoing star formation, for we only obtain redshifts for emission-line galaxies at these magnitudes.

We have checked that galaxies with spectroscopic redshifts are distributed uniformly over our field (see Figure 4); thus we do not need to apply a spatial completeness correction.

### 2.5.1 Sensitivity to Photometric Redshift Estimates

We repeat the calculations above, using the PDFs obtained from our empirical photo- $z$  measurements, described in § 2.4. We compare the resulting  $C_{SFR}$  and  $C_z$ , as a function of  $K$ , with our default measurements (described above) in Fig. 2. We find that the empirical photo- $z$  tends to return lower  $C_{SFR}$  and  $C_z$ , especially at  $22.5 \leq K \leq 24$ . The average  $C_z$  are [0.62, 0.43] for  $[22.5 < K, 22.5 \leq K \leq 24]$  using the empirical photo- $z$ , and are [0.68, 0.62] using the public photo- $z$ . The average  $C_{SFR}$  are [0.47, 0.77] and [0.41, 0.84] over the same magnitude ranges for using the empirical and public photo- $z$ , respectively. We note that none of our main results are sensitive to which completeness we choose, and we show this explicitly where relevant.

## 2.6 The SDSS comparison sample

The Sloan Digital Sky Survey (SDSS; York et al. 2000) is a project that has imaged  $10^4 \text{ deg}^2$  in  $u'g'r'i'z'$  passbands, and obtained spectra of  $10^6$  objects. Our sample is selected from Stripe 82, which is part of the SDSS ‘legacy survey’, and covers an area of  $275 \text{ deg}^2$ . Our catalog is generated using the method described in Gilbank et al. (2010a), and contains 47855 objects with  $r' < 19.5$  at  $0.032 \leq z \leq 0.2$ . The lower redshift boundary is set by the availability of the [OII] $\lambda 3727$  line. Each galaxy is assigned a completeness weight which is calculated using a method similar to that described in Baldry et al. (2005). The targeting completeness is nearly 100% at  $r' < 17.8$  and drops sharply at fainter magnitudes. We also match the objects in our sample to those in the SDSS DR4<sup>1</sup> to obtain stellar mass measurements, described in Kauffmann et al. (2003a). For those galaxies in DR7 but not in DR4, we derive their stellar mass use a color-based estimate of the mass-to-light ratio (e.g., Bell et al. 2003), fit empirically against the Kauffmann et al. (2003a) mass. The stellar mass obtained in this manner has  $1\sigma$  dispersion of 0.21 dex compared to the value of Kauffmann et al. (2003a).

Since we intend to use this SDSS sample to provide fiducial comparisons against our  $z \sim 1$  ROLES sample, we limit the catalogue in stellar mass to  $\log(M_*/M_\odot) > 8.5$ ; for star-forming galaxies our sample is complete for  $z < 0.05$ .

Gilbank et al. (2010a) demonstrated that Stripe 82 samples selected from [OII]-derived SFR are incomplete at high stellar mass. This is primarily because the detection of emission lines is sensitive to the contrast with the continuum; for the brightest galaxies, this imposes a selection limit in SFR which is not low enough to uncover all the star-forming galaxies at that magnitude. This problem is mitigated by using SFR derived from Balmer-decremented  $H\alpha$  measurements, since this is a stronger emission line (Gilbank et al. 2010a). We will therefore adopt this estimate of SFR for the SDSS sample. This still allows a fair comparison with our  $z \sim 1$  data, since the [OII]-derived SFR used there are empirically corrected to agree, on average, with the  $H\alpha$ -derived SFR.

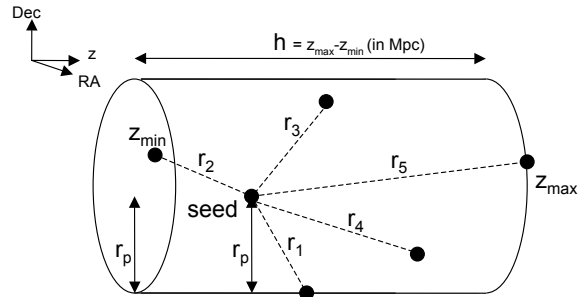


**Figure 3.** An illustration of a cylinder defined by the first five nearest neighbors of a target galaxy, for the purpose of computing local galaxy density.  $r_i$  with  $i=1,2,3,\dots,n$  are the 3D distances to each neighbor. The radius of the cylinder  $r_p$  is defined by the maximum projected distance of all these five nearest neighbors, while the height of the cylinder  $h$  is determined by the maximum redshift difference of the same galaxies.

## 3 LOCAL GALAXY DENSITY MEASUREMENTS

We will adopt a local galaxy density estimator,  $\rho_n$ , as a tracer of galaxy environment. This is an  $n^{\text{th}}$  nearest-neighbor method, counting galaxies with spectroscopic redshifts brighter than a specified luminosity. Our approach is to use the brighter galaxies to define the environment, as this sample is complete for both star-forming and passive galaxies, once weighted by  $1/C_z$ . Accordingly we consider galaxies with  $M_K \leq -21.0$  ( $\sim M_K^* + 2$ ) from the spectroscopic sample to define the environment. In section Appendix A we will consider the sensitivity of our results to this choice of density estimator.

For every galaxy in our full catalogue, the 3D angular diameter distances to its  $M_K \leq -21$  neighbours are computed; the distance in the  $z$ -direction is calculated using Eq. 19 in Hogg (1999). We compute the volume of a cylinder where the radius and height are determined from the first  $n$  nearest neighbors, as illustrated in Fig. 3. We use  $r_i$  to denote the 3D distance between the  $i^{\text{th}}$  nearest neighbor ( $M_K \leq -21$ ) and the target. The radius  $r_p$  of the cylinder is the maximum projected distance of  $r_i$  for all such neighbours at  $r_i \leq r_n$ , while the height  $h$  is determined from the maximum difference in  $z$  for the same nearest neighbors. We note that  $r_p$  is not necessarily the same as the projected distance of the  $n^{\text{th}}$  nearest neighbor in 3D, and the cylinder is not always centered at the target. Once  $r_p$  and  $h$  are determined,  $\rho_n$  is then computed as the total galaxy count  $N$  within this cylinder, which has volume  $V = \pi r_p^2 h$ . Here,  $N$  is computed by summing up the redshift completeness weights  $w_z (=1/C_z$ ; see §2.5) of all spectroscopic galaxies brighter than  $M_K = -21.0$  within the cylinder. That is,

$$\rho_n = \frac{\sum_{i=0}^n w_z(i)}{V}. \quad (3)$$

In calculating the volume of the cylinder, we correct for the area of its base if  $r_p$  extends beyond the survey limits. To do so, we first generate a random field mimicking our survey coverage, with a number density of  $3 \times 10^6$  random points per square degree. We then derive the area correction factor  $k_A$  as the ratio of the total number of the random points actually enclosed by  $r_p$  to the total expected number. The volume of the cylinder is accordingly adjusted as  $V = k_A(\pi r_p^2)h$ .

<sup>1</sup> <http://www.mpa-garching.mpg.de/SDSS/DR4/>

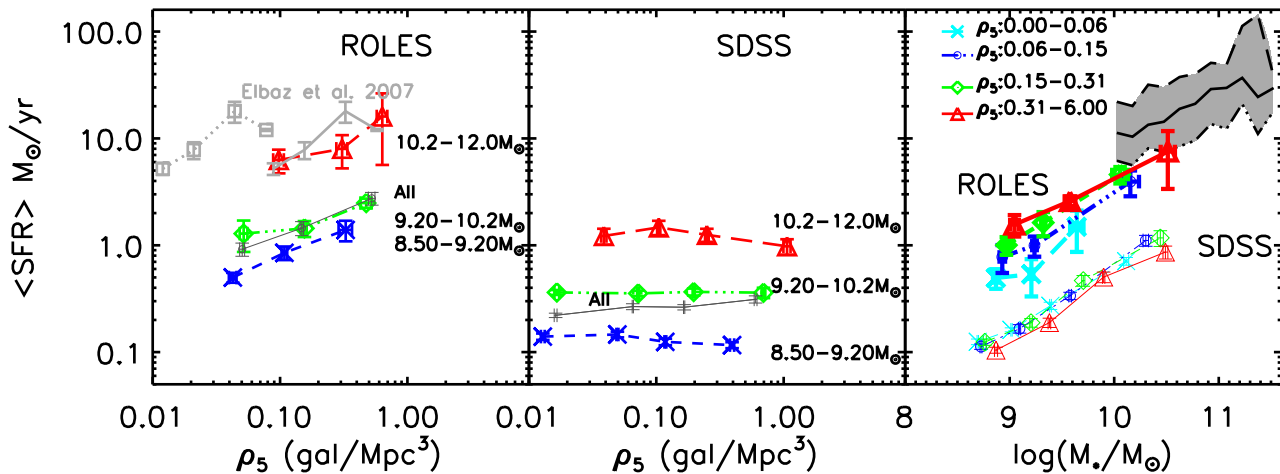


**Figure 5.** *Left and Middle:* The median SFR is shown as a function of  $\rho_5$  in each  $M_*$  bin, as indicated in the plot. The trend from the full sample, averaged over all masses, is overplotted as solid gray curve. The trend from Elbaz et al. (2007) is overplotted as the gray dotted curve in the ROLES panel, but shown as the gray solid one after multiplying their densities by an arbitrary factor of 7.4. Note their sample includes galaxies with  $M > 10^{10} M_\odot$ , so is most fairly compared with our red line. In each  $M_*$  bin, the SFR increases with  $\rho_5$  (marginally in the high  $M_*$  bin) in the ROLES sample, while there is no significant trend in the SDSS sample. *Right:* The median SFR as a function of  $M_*$  with  $\rho_5$  controlled. The gray shaded area is the “main sequence” with  $1\sigma$  uncertainty in SFR at  $z=0.98$  from Noeske et al. (2007b). The SFR increases with  $M_*$  in both ROLES and SDSS samples. The environmental density dependence is primarily observed for the lowest mass regime at  $z \sim 1$ ; no such dependence is present at  $z = 0$ .

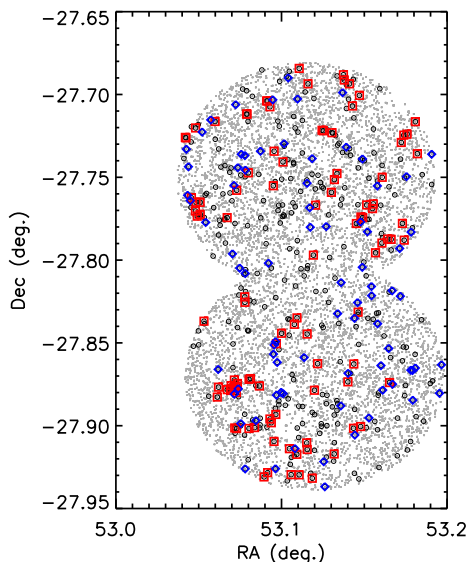


**Figure 4.** The spatial distribution of our spectroscopic sample in the CDFS. The gray dots are all galaxies in the photometric catalog, which demonstrates the geometry of our two-pointing LDSS3 configuration. Galaxies at  $0.889 \leq z_{spec} < 1.149$  are plotted in black open circles. Those located in the highest and lowest 20%  $\rho_5$  regions are marked by red squares and blue diamonds, respectively.

In Fig. 4 we present the spatial distribution of our spectroscopic sample, where all galaxies at  $0.889 \leq z < 1.149$  are plotted as black circles. Galaxies located within the highest and lowest 20%  $\rho_5$  regimes are marked by the red squares and blue diamonds, respectively. We can see that the galaxies identified as high-density regions are the most clustered, suggesting that our density estimator

is reasonable. We will test this further, in the following subsection. Finally, we note that our choice of a 3D, nearest-neighbour density estimator is one of several density estimators that have been used in the literature. In Appendix A3, we will explore how our conclusions might be influenced by different choices.

## 4 RESULTS

We intend to study the interplay between stellar mass and local galaxy density, as they affect the average SFR and sSFR of star-forming galaxies. In all the following analysis, star-forming galaxies are selected from the ROLES  $z \sim 1$  sample by requiring a detection of [OII] emission. In the  $z = 0$  comparison Stripe 82 sample, we require  $sSFR > 5 \times 10^{-12} \text{yr}^{-1}$ , which we find provides a good separation between the red sequence and blue-cloud population. All results use weights that are based on the FIREWORKS photo- $z$ ; we have checked that our conclusions are unchanged if we repeat the analysis using our empirical photo- $z$  measurements.

### 4.1 The correlation between SFR, mass and environment

In Fig. 5 we plot the median SFR as a function of  $\rho_5$  for both the ROLES and SDSS samples. First, we consider the average trend, including all star forming galaxies regardless of their mass; this is shown as the thin, grey, solid curves. Locally, there is no significant trend with environment, as expected. At  $z = 1$ , however, we find that the median SFR in our densest regions is a factor  $\sim 3$  larger than in the lowest-density regions. The SFRs in our ROLES sample are about  $\sim 10$  times larger than those in the SDSS sample in the high  $\rho_5$  regime, but only a factor of  $\sim 4$  in the low  $\rho_5$  regions.

This echoes the recently discovered ‘reverse’ SFR–density relation at  $z \sim 1$  (e.g. Elbaz et al. 2007; Cooper et al. 2008; Ideue et al. 2009). We compare our data directly with those of



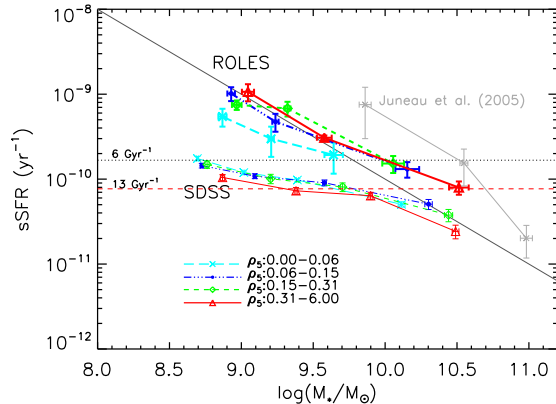


**Figure 6.** We show the sSFR for star forming galaxies as a function of  $\log(M_*)$ , in different bins of density  $\rho_5$ , for the ROLES ( $z = 1$ , thick line) and SDSS  $z < 0.05$  (thin line) samples. The solid diagonal line has  $\text{SFR} = 1 M_\odot/\text{yr}$ . The horizontal dotted and short dashed lines represent  $t=6$  and 13 Gyr, corresponding to the age of the Universe at  $z \sim 1$  and  $z = 0$ , respectively. The data of Juneau et al. (2005) are overplotted as the gray, solid curve for comparison. The sSFR at fixed  $\rho_5$  decreases with  $\log(M_*)$  in the both samples. The lowest sSFR is observed in the lowest  $\rho_5$  bin in the ROLES  $z \sim 1$  sample. Locally, the SDSS sample shows little trend with  $\rho_5$ ; if anything, the sSFR is lowest in the highest density environments.

Elbaz et al. (2007), by showing their results as the gray dotted curve in Fig. 5. In Appendix A3 we show that their density estimate is not directly comparable to ours, and in particular is less sensitive to environment for our particular sample. Based on the results of this comparison, we have arbitrarily scaled their densities by a factor of 7.4. The magnitude of the trend we observe, for comparably massive galaxies  $M < 10^{10} M_\odot$ , is comparable to that of Elbaz et al. (2007).

We also show our results divided into different stellar mass bins, in the same figure. Interestingly, the same conclusions hold for all mass bins: while there is little or no trend of SFR with density locally, we see a significant increase at  $z = 1$ . The trend appears to be strongest for the lowest-mass galaxies, however.

The right panel of Fig. 5 summarizes the SFR–density relation, now presented as SFR as a function of stellar mass. Overall, we see the expected increase in SFR with stellar mass, at both epochs, as has been noted by many others. For example, we show the “main sequence” of star-forming galaxies at  $0.85 < z < 1.0$  as measured by Noeske et al. (e.g. 2007b) as the gray shaded area in Fig. 5. Their data, which use  $24\mu\text{m}$  luminosities to estimate SFR, show a similar trend but higher normalization compared with our data. We will explore this relation in more detail in a forthcoming paper (Paper IV; Gilbank et al., in prep). For now we are interested in the environmental dependence, and we divide this relation into bins of  $\rho_5$ , as indicated on the figure. The choice of  $\rho_5$  bins in the ROLES sample is determined by requiring a similar number of galaxies in each  $\rho_5$  bin, and we choose the same bins when considering the SDSS sample. Both the ROLES and SDSS samples show an increasing median SFR with larger  $M_*$  in all environments, and the ROLES sample always has higher SFR than the SDSS. Again we observed that the lowest mass galaxies at  $z = 1$  show a significantly higher SFR in denser environments, while there is little or no trend locally.

Because massive galaxies possess higher SFR than low-mass galaxies due to their larger integrated gas content, the sSFR pro-

vides a better understanding of SFR efficiency. The sSFR is known to decline with increasing stellar mass both in low- and high- $z$  galaxies, as an outcome of gradual decreasing SFR in galaxies (e.g., Noeske et al. 2007a,b; Oliver et al. 2010). Thus, in Figure 6, we show sSFR as a function of stellar mass and  $\rho_5$ ; both ROLES and SDSS show that the sSFR decreases with  $M_*$ . The ROLES sample exhibits higher sSFR than the SDSS sample at a fixed  $M_*$ , and the difference is more significant for lower stellar masses. We can interpret the sSFR as a ratio of current SFR to the past-average SFR. In the Figure we plot horizontal lines indicating the age of the Universe at  $z \sim 1$  (gray dotted line) and  $z \sim 0$  (red short dashes). Galaxies below these lines are inefficient in forming stars, i.e. their current SFR is much less than their past average. Galaxies above the lines are more active and would be interpreted as having a current burst of SFR such that it exceeds the past average. The separation between the ‘active’ and ‘passive’ SFR regimes occurs at  $\log(M_*/M_\odot) \sim 10$  at  $z \sim 1$  but at  $\log(M_*/M_\odot) \sim 9.6$  at  $z \sim 0$ , showing a mass dependence in the sense that that the contributors of SFR have shifted toward lower  $M_*$  as redshift decreases. This provide evidence for down-sizing in SFR in the respect of the ‘cross-over’ time between the ‘active’ and ‘passive’ SFR regimes. This accords with previous work such as that of Juneau et al. (2005), which is overplotted as the gray solid curve, with the SFR recomputed using the mass-dependent correction in Paper II. However unlike that work, our census is complete at  $z \sim 1$  for galaxies with masses below the cross-over mass. We explore this further in Paper IV (Gilbank et al. in prep).

Dividing the samples by  $\rho_5$ , we find that the evolution of this cross-over time holds in all environments. Only the lowest-mass star-forming galaxies at  $z = 1$  (less than  $\sim \log(M_*/M_\odot) = 9.5$ ) exhibit an increasing sSFR with  $\rho_5$ . No such dependence is seen in the local comparison sample; if anything, there is a mild *decrease* in the mean sSFR at the highest densities, locally (see also, e.g. Balogh et al. 2004; Patel et al. 2009; Rines et al. 2005; Balogh et al. 2009). In other words, the lowest-mass star-forming galaxies in high-density regions have the largest decrease in sSFR from  $z=1$  to  $z \sim 0$ . This suggest that the evolution of galaxies with  $M < 10^{10} M_\odot$  is characterised by a more rapid decrease of star formation in moderately dense regions.

## 4.2 Star formation density

Paper II presented the dependence of SFR density ( $\rho_{\text{SFR}}$ ) on stellar mass in the ROLES survey, finding the same shape as seen in the local SDSS. In Fig. 7 we now extend this to show  $\rho_{\text{SFR}}$  as a function of  $M_*$  in different environments, as measured by  $\rho_5$ . The  $\rho_{\text{SFR}}$  in each  $M_*$  bin is computed following Paper II as

$$\rho_{\text{SFR}} = \sum_i \frac{w_{\text{SFR},i} \text{SFR}_i}{V_{\text{max},i}},$$

where  $w_{\text{SFR},i} = 1/C_{\text{SFR},i}$  (see §2.5) and  $V_{\text{max},i}$  is the maximum volume in which galaxy  $i$  could be located and have been found as  $K \leq 24$  and  $0.889 \leq z \leq 1.149$ .

Including galaxies in all environments, our results in the top-left panel in Fig. 7 are consistent with those of Paper II. We next present this same distribution in different  $\rho_5$  bins, with results shown also in Fig. 7. The trends are noisy, especially for the ROLES sample, due to the small sample size in each  $\rho_5$  and  $\log(M_*)$  bin. Nonetheless, we see that, in the local sample, the lowest-mass galaxies ( $\log(M_*/M_\odot) < 9.5$ ) tend to exhibit a decreasing  $\rho_{\text{SFR}}$  with increasing density. At higher masses, there is

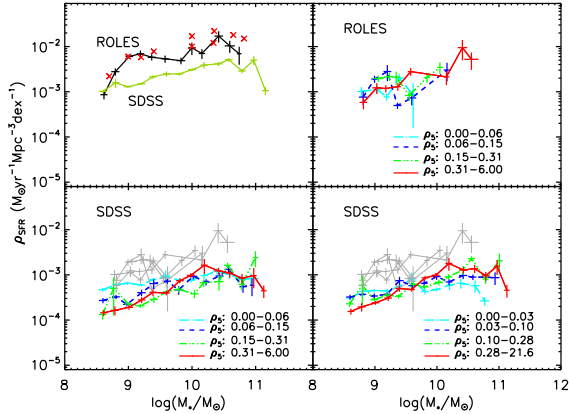


**Figure 7.** The SFRD is shown as a function of  $\log(M_*/M_\odot)$ , using a bin size of  $\Delta\log(M_*/M_\odot)=0.2$ . In the top-left panel, galaxies in all  $\rho_5$  bins are combined together for the ROLES ( $z \sim 1$ , black) and SDSS  $z < 0.05$  (green) samples. The data of the  $z \sim 1$  sample in Paper II are overplotted as red crosses. The top-right panel shows the same data, divided into bins of different environment, as measured by  $\rho_5$ . The results for the SDSS are presented in the bottom two panels. In the lower-left panel, the  $\rho_5$  bins are chosen to exactly match those in ROLES; in the right panel we choose the  $\rho_5$  bins to include an equal number of SDSS galaxies in each bin. The gray curves in each SDSS panel are the ROLES results from the top-right panel, for comparison. The ROLES sample exhibits a larger SFRD at all stellar masses than the SDSS sample, reflecting the decline of global SFRD. Little or no environmental dependence is observed at  $z = 1$ , which suggests that the small trend we observe — for low-mass galaxies to have higher SFR in denser regions — has little effect on the global SFRD.

little or no dependence on environment. In our  $z = 1$  ROLES sample, there is no clear dependence of  $\rho_{SFR}$  on environment. The small increase we see in median SFR toward higher densities appears to have little noticeable impact on the total SFR density.

The evolution we see indicates that environment accelerates quenching of the lowest-mass galaxies with time, but that  $\rho_{SFR}$  is governed primarily by the stellar mass of the galaxy.

## 5 DISCUSSION AND CONCLUSIONS

We have used our highly sensitive, complete LDSS3 spectroscopy in the CDFS field to probe the effects of environment on galaxy evolution at  $z = 1$ , for galaxies with masses lower than have ever been probed in this way before. We consider only star-forming galaxies, for which our survey, and  $z = 0$  comparison sample, are complete for stellar masses  $M > 10^{8.5} M_\odot$ . Locally, star-forming galaxies show little dependence on environment. Specifically, the correlation between SFR and mass, or between sSFR and mass, shows no dependence on local density. The situation is quite different at  $z = 1$ , where we find SFR and sSFR is actually somewhat *larger* in dense environments. Thus we confirm the general trend found by others (e.g. Elbaz et al. 2007; Muzzin et al. 2008; Cooper et al. 2008; Ideue et al. 2009); moreover, we find that this trend is stronger for galaxies with masses below those studied in previous work. This has little effect on the total SFR density however which, at fixed stellar mass, shows no clear trend with environment.

In summary, we find that the decline in SFR-mass and sSFR-mass relations from  $z \sim 1$  to  $z \sim 0$  depends on environment, with a faster decline in richer environments. Note that, due to the small

field size, our sample does not include the densest environments, such as the cores of rich clusters. Recent results from Sobral et al. (2010) suggest that it is in these intermediate density environments that star formation may be most enhanced, at  $z \sim 1$ .

However these effects are small when compared to the intrinsic dependence of SFR and sSFR on mass itself. In agreement with other studies, we conclude that mass is the dominant variable, driving the history of star-formation (e.g. Peng et al. 2010; Iovino et al. 2010; Cucciati 2010). Environment appears to play a secondary role, albeit one that is more important for lower-mass galaxies. This may be expected, since the smaller gas reservoir of less massive galaxies may be more easily affected by environment. Mechanisms such as galaxy mergers and harassment are more likely in denser environments, and these may enhance the star formation activity within the galaxies, resulting in the positive SFR- $\rho_5$  and sSFR- $\rho_5$  trend we see at  $z \sim 1$ . Since such vigorous star formation will speed up the consumption of cold gas within the galaxies, they would more quickly exhaust their gas supply. At later times, the star-formation rates would be then be *less* than the counterparts in poorer environments.

While this work is among the first to spectroscopically probe the low-mass regime at  $z \sim 1$ , it suffers from limitations that can be addressed in future work. The main one is statistics: error bars can be greatly improved by larger area, future surveys. Also ROLES lacks sufficient volume to probe the densest environments (rich clusters) in which the most massive galaxies are found; interesting, recent work by Sobral et al. (2010) suggests that the enhancement in SFR we find may not appear in such massive clusters. Wider, or cluster-targetted, surveys in the future will be able to address this. Future papers based on ROLES will explore the lower redshift regime in our survey. This will allow evolution to be explored further but also more extreme environments to be probed. This is possible because the FIRES patch contains a massive cluster, MS1054-03, at  $z=0.83$ , and the CDFS patch exhibits a large-scale filament (and galaxy groups) at  $z=0.73$ .

Our work is based on a key assumption, that the mass-dependent conversion from [OII] to SFR derived in the local universe by Gilbank et al. (2010a) can be applied to  $z \sim 1$ . As dust plays an important role in deriving SFR from [OII] flux, further inspection will be made using  $24\mu\text{m}$  and radio data in the future (Gilbank et al., in prep). However, in general, low-mass galaxies contain little dust and hence are undetected in those bands. Since our key results lie in low-mass galaxies, and we are comparing trends at a fixed stellar mass, any systematics related only to mass should not affect our results about the relative star formation rates in different environments.

Finally we note that our work has focused on using local density estimators as a simple proxy for environment. An alternative approach worth pursuing would be to use linking algorithms to try and identify actual physical galaxy groups. This may allow a better connection from observables to theoretical concepts such as halo and sub-halo masses.

## 6 ACKNOWLEDGMENTS

This paper includes data gathered with the 6.5-m Magellan Telescopes located at Las Campanas Observatory, Chile. We thank LCO and the OCIW for the allocation of time to this project as part of the LDSS3 instrument project. Australian access to the Magellan Telescopes was also supported through the Major National Research Facilities and the National Collaborative Research Infras-



structure Strategy programs of the Australian Federal Government. KG and I.H.L. acknowledge financial support from Australian Research Council (ARC) Discovery Project DP0774469. MLB acknowledges support from the province of Ontario in the form of an Early Researcher Award.

## REFERENCES

- Abraham et al., R. G. 2004, *AJ*, 127, 2455
- Baldry, I. K., Balogh, M. L., Bower, R. G., Glazebrook, K., Nichol, R. C., Bamford, S. P., & Budavari, T. 2006, *MNRAS*, 373, 469
- Baldry, I. K., & Glazebrook, K. 2003, *ApJ*, 593, 258
- Baldry et al., I. K. 2005, *MNRAS*, 358, 441
- Balogh, M. L., Baldry, I. K., Nichol, R., Miller, C., Bower, R., & Glazebrook, K. 2004, *ApJL*, 615, L101
- Balogh et al., M. 2004, *MNRAS*, 348, 1355
- Balogh et al., M. L. 2009, *MNRAS*, 398, 754
- Bamford et al., S. P. 2009, *MNRAS*, 393, 1324
- Bell, E. F., McIntosh, D. H., Katz, N., & Weinberg, M. D. 2003, *ApJS*, 149, 289
- Bell, E. F., Zheng, X. Z., Papovich, C., Borch, A., Wolf, C., & Meisenheimer, K. 2007, *ApJ*, 663, 834
- Blanton et al., M. R. 2003, *ApJ*, 592, 819
- Carter, B. J., Fabricant, D. G., Geller, M. J., Kurtz, M. J., & McLean, B. 2001, *ApJ*, 559, 606
- Cassata et al., P. 2007, *ApJS*, 172, 270
- Cimatti et al., A. 2002, *A&A*, 381, L68
- Cooper, M. C., et al. 2010, *ArXiv e-prints*
- Cooper et al., M. C. 2008, *MNRAS*, 383, 1058
- Cowie, L. L., Songaila, A., Hu, E. M., & Cohen, J. G. 1996, *AJ*, 112, 839
- Cucciati, O. e. a. 2010, *ArXiv e-prints*
- Daddi et al., E. 2002, *A&A*, 384, L1
- Davies et al., G. T. 2009, *MNRAS*, 395, L76
- Dressler, A. 1980, *ApJ*, 236, 351
- Elbaz et al., D. 2007, *A&A*, 468, 33
- Förster Schreiber et al., N. M. 2006, *AJ*, 131, 1891
- Gilbank, D. G., Baldry, I. K., Balogh, M. L., Glazebrook, K., & Bower, R. G. 2010, *MNRAS*, 405, 2594 (a)
- Gilbank et al., D. G. 2010, *MNRAS*, 405, 2419 (b)
- Glazebrook, K., & Bland-Hawthorn, J. 2001, *PASP*, 113, 197
- Glazebrook et al., K. 2004, *Nature*, 430, 181
- Gómez et al., P. L. 2003, *ApJ*, 584, 210
- Hildebrandt, H. e. a. 2010, *ArXiv e-prints*
- Hogg, D. W. 1999, *ArXiv Astrophysics e-prints*
- Hogg et al., D. W. 2004, *ApJL*, 601, L29
- Hopkins et al., A. M. 2004, *ApJ*, 615, 209
- Ideue et al., Y. 2009, *ApJ*, 700, 971
- Iovino et al., A. 2010, *A&A*, 509, A40+
- Jansen, R. A., Franx, M., & Fabricant, D. 2001, *ApJ*, 551, 825
- Juneau et al., S. 2005, *ApJL*, 619, L135
- Kauffmann, G., White, S. D. M., Heckman, T. M., Ménard, B., Brinchmann, J., Charlot, S., Tremonti, C., & Brinkmann, J. 2004, *MNRAS*, 353, 713
- Kauffmann et al., G. 2003a, *MNRAS*, 341, 33
- . 2003b, *MNRAS*, 341, 54
- Kennicutt, Jr., R. C. 1998, *ARA&A*, 36, 189
- Kewley, L. J., Geller, M. J., & Jansen, R. A. 2004, *AJ*, 127, 2002
- Lewis et al., I. 2002, *MNRAS*, 334, 673
- Li, I. H., & Yee, H. K. C. 2008, *AJ*, 135, 809
- Li, I. H., Yee, H. K. C., & Ellingson, E. 2009, *ApJ*, 698, 83
- Lilly, S. J., Le Fevre, O., Hammer, F., & Crampton, D. 1996, *ApJL*, 460, L1+
- Lilly et al., S. J. 2007, *ApJS*, 172, 70
- Madau, P., Ferguson, H. C., Dickinson, M. E., Giavalisco, M., Steidel, C. C., & Fruchter, A. 1996, *MNRAS*, 283, 1388
- Magnelli, B., Elbaz, D., Chary, R. R., Dickinson, M., Le Borgne, D., Frayer, D. T., & Willmer, C. N. A. 2009, *A&A*, 496, 57
- Maier, C. e. a. 2009, *ApJ*, 694, 1099
- Mobasher et al., B. 2004, *ApJL*, 600, L167
- . 2009, *ApJ*, 690, 1074
- Muzzin, A., Wilson, G., Lacy, M., Yee, H. K. C., & Stanford, S. A. 2008, *ApJ*, 686, 966
- Noeske et al., K. G. 2007a, *ApJL*, 660, L47
- . 2007b, *ApJL*, 660, L43
- Oliver et al., S. 2010, *MNRAS*, 588
- Pannella et al., M. 2009, *ApJ*, 701, 787
- Patel, S. G., Holden, B. P., Kelson, D. D., Illingworth, G. D., & Franx, M. 2009, *ApJL*, 705, L67
- Peng et al., Y. 2010, *ArXiv e-prints*
- Pozzetti, L. e. a. 2009, *ArXiv e-prints*
- Rines, K., Geller, M. J., Kurtz, M. J., & Diaferio, A. 2005, *AJ*, 130, 1482
- Santini et al., P. 2009, *A&A*, 504, 751
- Sobral, D., Best, P., Smail, I., Geach, J., Cirasuolo, M., Garn, T., & Dalton, G. B. 2010, *ArXiv e-prints*
- Vanzella et al., E. 2005, *A&A*, 434, 53
- . 2006, *A&A*, 454, 423
- . 2008, *A&A*, 478, 83
- Vogt et al., N. P. 2005, *ApJS*, 159, 41
- von der Linden, A., Wild, V., Kauffmann, G., White, S. D. M., & Weinmann, S. 2010, *MNRAS*, 404, 1231
- Vulcani, B., Poggianti, B. M., Finn, R. A., Rudnick, G., Desai, V., & Bamford, S. 2010, *ApJL*, 710, L1
- Wuyts, S., Labbé, I., Schreiber, N. M. F., Franx, M., Rudnick, G., Brammer, G. B., & van Dokkum, P. G. 2008, *ApJ*, 682, 985
- Yee, H. K. C., Hsieh, B. C., Lin, H., & Gladders, M. D. 2005, *ApJL*, 629, L77
- York et al., D. G. 2000, *AJ*, 120, 1579

## APPENDIX A: TESTS OF LOCAL GALAXY DENSITY

In this Appendix, we explore the sensitivity of our main results to our choice of density estimator. Our measurement of environment is an estimator based on a biased, incomplete tracer population, and we expect that its correlation with a fundamental quantity (such as dark matter density field) will be both biased and noisy. We will not attempt to directly connect our estimates directly to more physical parameters like these; however, we will ensure that we are able to distinguish high-density environments from low. To do this, we will use the local SDSS sample, which benefits from both large area and high spectroscopic completeness. We first apply our computation of  $\rho_n$  to the SDSS sample described in § 2.6, and compare with the density estimates of Baldry et al. (2006). The latter are computed based on a 2D,  $n^{th}$ -nearest-neighbor method, for galaxies limited to  $M_{r'} = -20 - Q(z - z_0)$  with  $Q=1.6$  and  $z_0=0.05$  from Blanton et al. (2003). The local galaxy density  $\Sigma_5$  is calculated from the projected distance to the 5<sup>th</sup> nearest neighbor, within a redshift slice of  $\Delta cz=1000\text{km/s}$  centered at each seed galaxy. By comparison with simulations and models, Baldry et al. (2006) show that  $\Sigma_5$  correlates well with the smoothed, dark matter

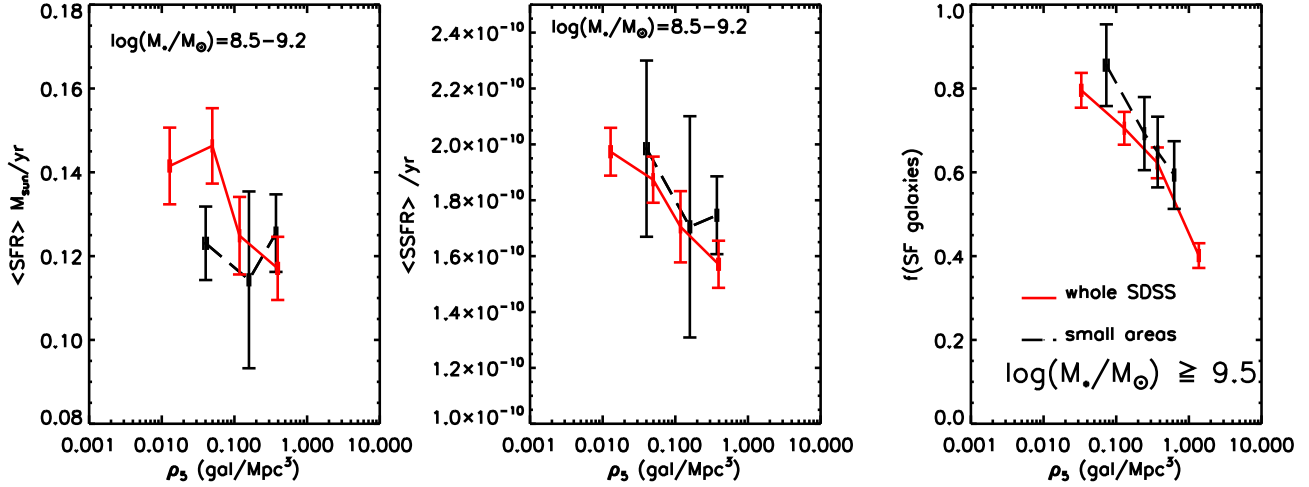


**Figure A1.** To test our measure of environment, we use the SDSS Stripe 82 sample. We select random regions with a similar physical size to one of our LDSS3 pointings at  $z = 1$ , and measure the local density  $\rho_5$ . We then combine those 28 fields that have an average density equal to the average density in our ROLES field, to within 20 per cent. The *Left* and *Middle* panels show the SFR- and sSFR- $\rho_5$  trends for star-forming galaxies with  $\log(M_*/M_\odot)=8.5-9.2$  at  $z \leq 0.05$  from this experiment, as the black line. This is compared with the result obtained from the full Stripe 82 sample, shown as the thick red curve. No strong trend with environment is seen in any case. The right panel is similar, but for the fraction of star-forming galaxies with  $\log(M_*/M_\odot) \geq 9.5$ . Here, the well-known trend with environment is recovered, even with small field sizes. Thus, we conclude that our survey is large enough to detect environmental trends like those present at  $z = 0$ .

overdensity. We will therefore take this as our best estimate of the “true” density in the SDSS, and in the following subsection we will compare how our methods and sample limitations compare with this.

### A1 Sensitivity to the limited field size

Likely the biggest limitation of our  $z = 1$  sample, is the field size (see discussion in Cooper et al. 2010). Our LDSS3 spectroscopic coverage of CDFS is comprised of two adjacent, circular fields with diameter  $8.3'$ , corresponding to  $\sim 4.1$  Mpc at  $z \sim 1$ . Thus, we do not expect a large dynamic range of environment within our sample. Moreover, our density estimator  $\rho_n$  effectively smooths this density field over fairly large scales. The choice of using smaller  $n$  results in higher resolution, but a noisier density estimate; on the other hand, a larger  $n$  reduces the difference between the extreme high and low density regions and smears out any trends which depend on local galaxy density. Edge corrections also become more important for larger choices of  $n$ . With our default choice of  $n=5$ , the median  $r_p$  is  $\sim 2.6$  Mpc ( $\sim 5.4'$  at  $z=1$ ) and  $h$  is  $\sim 3.8$  Mpc ( $\Delta z \sim 0.003$ ). The spatial component is thus actually larger the size of our field for median densities; thus, most of the sensitivity comes from the redshift dimension. Nonetheless, as we will show, it is still possible to distinguish high- and low-density environments.

We carry out the test by randomly choosing 500 circular regions from the SDSS Stripe 82 sample, each with a diameter of 4.1 Mpc at  $z=0.05$ . Thus, the field size is matched to the same physical area covered by a single LDSS3 pointing at  $z = 1$ . In each field we compute  $\rho_n$  with  $n=[3,5,7]$ . Forty of these 500 circular regions are rejected because their mean  $\rho_n$  are significantly larger than that in ROLES. The computed  $\rho_n$  for these SDSS galaxies have a  $1\sigma$  dispersion of [0.46, 0.22, 0.08], and the median  $r_p$  are [1.39, 2.16, 2.8] Mpc for  $n=[3,5,7]$ . We compare these  $\rho_n$ , computed within the limited field size, with our best estimate of the “true” density field,  $\Sigma_5$ . We find a  $1\sigma$  dispersion between  $\rho_n$  and  $\Sigma_5$  are [0.67, 0.49, 0.47]

dex for  $n=[3,5,7]$ . Thus, for our default choice of  $n = 5$ , we can hope to distinguish environments separated by  $\sim 1$  dex with  $2\sigma$  confidence. We will show that our  $z = 1$  sample spans a factor of  $\sim 100$  in  $\rho_5$ ; thus we anticipate that differences between the highest and lowest-density environments in that sample will be meaningful.

We proceed to check this further, by comparing our measurement of  $\rho_5$  in SDSS with quantities that have known environmental trends. In particular, we will consider the SFR and the specific SFR (sSFR), the relevant quantities for our  $z = 1$  analysis. To improve the statistics, we stack the 28 circular regions that have an average density within 20% of each other, and comparable to the average density in our  $z = 1$  sample. This ensures that we have enough galaxies to reliably measure average galaxy properties, and that the dynamic range of density probed will be comparable to what we can expect from our survey. Note the stacking does not reduce the noise, or potential bias, in our density estimate, since these estimates are still made on the individual fields.

We show the average SFR and sSFR as a function of  $\rho_n$  with  $n=5$  in the stacked regions in Fig. A1. We only include star-forming galaxies here, by selecting those with  $sSFR > 5 \times 10^{-12} \text{yr}^{-1}$ . This effectively removes passive, red-sequence galaxies from the sample. We also limit this test to galaxies with  $\log(M_*/M_\odot)=8.5-9.2$ , which is the mass range of primary interest in this paper. In both cases, there is little trend with environment; this result is expected since we are only considering the star-forming population. This demonstrates that systematics in our density estimator do not induce an artificial correlation in sSFR.

The next test is to consider the fraction of star-forming galaxies ( $sSFR > 5 \times 10^{-12} \text{yr}^{-1}$ ) in the SDSS, since this is known to correlate strongly with density. Here, we need to consider a sample limited at a higher stellar mass,  $\log(M_*/M_\odot) \geq 9.5$ , because the passive galaxy population becomes incomplete below that limit. We show this fraction as a function of  $\rho_5$ , limited to small fields as before, as the black dashed curve in the right panel of Fig. A1. Again, this is compared with the trend obtained using the full sur-

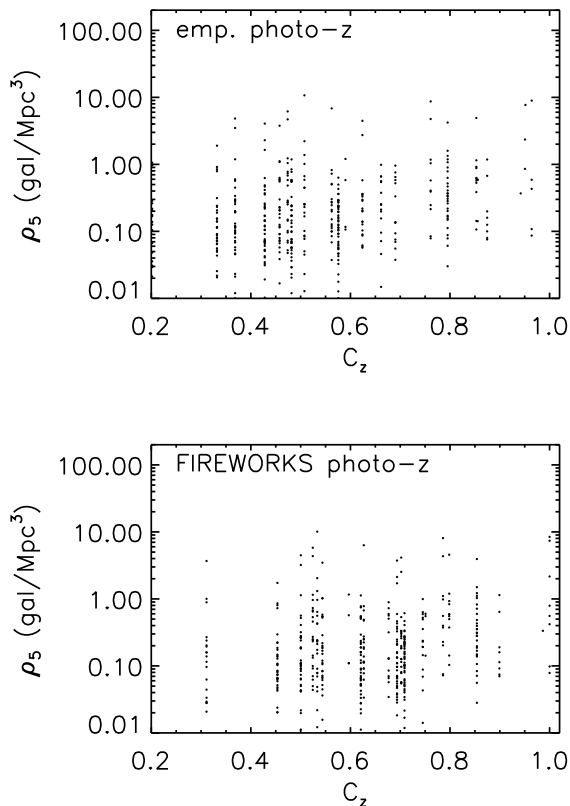


**Figure A2.** The local galaxy density  $\rho_5$  is shown as a function of redshift completeness  $C_z$  for galaxies at  $0.889 \leq z \leq 1.149$ . Completeness are estimated using either our empirical (*top*) photo-z, or the public FIREWORKS (*bottom*) photo-z. We find that  $\rho_5$  is not a strong function of  $C_z$ , and is not sensitive to our photo-z estimate.

vey area, shown as the red curve. We see that a strong environmental dependence is still observed from the limited field areas, with surprisingly little evidence for any bias or smoothing of the trend. Therefore, we conclude that despite the small field, our choice of density measure is robust and able to differentiate truly different environments, as also suggested in Figure 4.

## A2 Sensitivity to incompleteness

Next, we consider the effect of our completeness weights, and their sensitivity to the photo-z estimates (which is the only place the photo-z play a role in our analysis). We examine how the choice of photo-z method might affect our computation of  $\rho_n$  in Fig. A2, where we choose  $n = 5$ , and plot  $\rho_5$  as a function of redshift completeness ( $C_z$ ). Regardless of which photo-z method is used,  $\rho_n$  is not a strong function of redshift completeness. The *rms* dispersion between the two measurements of  $\rho_5$ , on a galaxy-by-galaxy basis, is  $\sim 0.025$  dex. Thus we find that  $\rho_5$  is fairly insensitive to the completeness correction, and thus to which photo-z method is used.

We now consider whether  $\rho_5$  itself is biased in the presence of spectroscopic incompleteness. The exercise is conducted by applying a spectroscopic incompleteness to our SDSS Stripe 82 sample, which is similar to the  $C_z$  in ROLES. To do so, we take the  $C_z$  as a function of  $K$  in Fig.2 (the FIREWORKS curve), and then convert

it into a function of  $r'$  based on the magnitude relative to  $M^*$ . We use  $m_K^* = 20.34$  and  $m_{r'}^* = 17.26$ . This produces a  $C_z$  that starts to drop from 1 at  $r' = 16$  to  $C_z \sim 0.52$  at  $r' = 19.0$ . Galaxies are then removed randomly in each magnitude in to satisfy the ‘expected’  $C_z$  in that magnitude bin. The original completeness in the SDSS sample is also accounted for during this process. The re-computed  $\rho_5$  correlates well with the original (complete)  $\rho_5$  estimate, with a  $1\sigma$  dispersion of only  $\sim 0.02$ . We find no evidence for a bias at high or low densities from this experiment.

From these tests we conclude that our  $\rho_5$  measure is robust, and a reasonable proxy for galaxy environment in our sample.

## A3 Sensitivity to choice of environment tracer

Our choice of a 3D, nearest-neighbour density estimator is one of several density estimators that have been used in the literature. In this subsection, we will explore how are results would be affected if we adopted a different method. We thus consider the SFR and sSFR of our lowest-mass galaxies in the  $z = 1$  sample,  $8.5 < \log(M_*/M_\odot) < 9.2$ . Figure A3 shows how this depends on density for the variety of possible choices we will explore below, compared with our default choice of  $\rho_5$ .

First, we consider the sensitivity to the smoothing length by considering the effect of different choices of  $n$ , by showing results for  $n = 3, 5$  and  $7$  in Figure A3. In all three cases we observe that the average sSFR and sSFR of the star-forming population *increases* with increasing density. This, our main result, is not sensitive to the choice of  $n$ .

Next, we consider the effect of using a cylinder of fixed volume to compute density. This has the advantage that the smoothing scale does not depend on density, but has the disadvantage that the noise in the estimator does depend on density. We choose a fixed cylinder with  $r_p = 2.6$  Mpc and  $h = 3.8$  Mpc, and re-compute the density. The density is then computed as the sum of  $w_z$  of galaxies within the cylinder divided by the cylinder volume, including a correction for edge effects. We denote this density as  $\rho_{fixed}$ , and show the results in Fig. A3. Again, the trend of increasing sSFR and with density is unchanged; however the correlation between SFR and density has become insignificant. This is likely due to the fact that a fixed volume results in a large uncertainty in the lowest-density regions, as can be seen by the larger error bars of this measure in Figure A3.

Elbaz et al. (2007) compute a density within a comoving box, with dimension of  $1.5 \times 1.5 \times 40$  Mpc ( $= 90 \text{ Mpc}^3$ ). Since we compare our SFR–density relation to theirs in §4, we calculate this density for our sample, and label it  $\rho_{90}$  in Fig. A3. The resulting densities are approximately an order of magnitude smaller than  $\rho_5$ , and no correlation with SFR or sSFR is observed. This is because we have too few spectroscopic density tracers to sufficiently populate the fixed box size. Thus it is not feasible for us to use this definition for our sample.

An alternative option is to use a 2D, projected density. This is widely used in the literature, and we adopt the method described in Baldry et al. (2006). We explore the effect of making two redshift slices of  $\Delta \frac{cz}{1+z} = 500$  and  $1000$  km/s. Within each redshift slice centered, at a target, galaxy, the local galaxy density is computed based on the projected distance to the nearest  $5^{th}$  neighbor. The SFR– and sSFR–density relations using these projected densities are also presented in Fig. A3. The same trend we detect in  $\rho_5$  is apparent using these projected estimators.

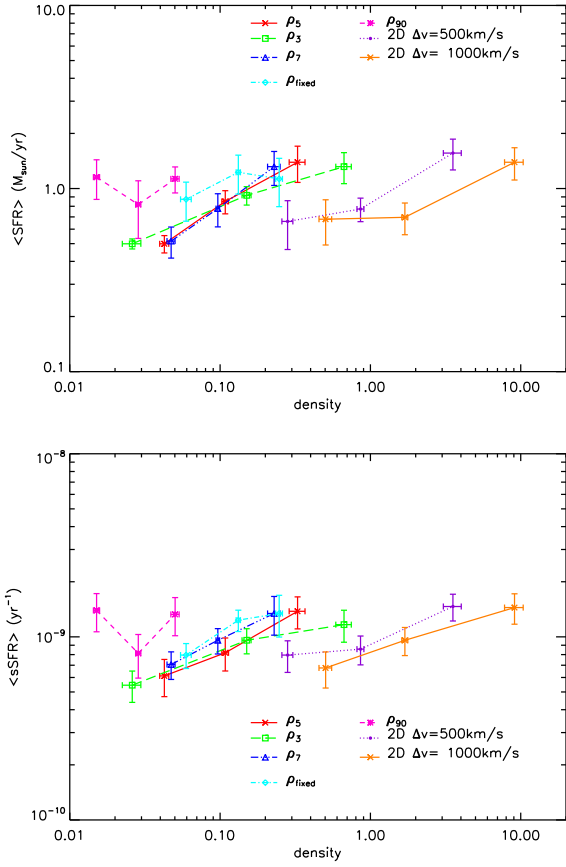


**Figure A3.** The SFR– and sSFR–density trends are shown, for the ROLES sample at  $z = 1$ . The densities are computed with the various methods described in this Appendix, as indicated in the plots. Only galaxies with  $\log(M_*/M_\odot)=8.5-9.2$  are used in plotting the SFR– and sSFR–density relation. The conclusions that both SFR and sSFR increases with density remain for most choices of densities. The only exception is  $\rho_{90}$ , which is chosen to match the fixed–volume density estimate of Elbaz et al. (2007); our spectroscopic sample of environment tracers is too sparse to yield a useful environment measurement with that definition.